Rock Mechanics and Rock Engineering (2021) 54:2067–2078
https://doi.org/10.1007/s00603-020-02358-y

TECHNICAL NOTE

Estimating the Uniaxial Compressive Strength of Argillites Using Brazilian Tensile Strength, Ultrasonic Wave Velocities, and Elastic Properties

U. C. Iyare[1] · O. O. Blake[1] · R. Ramsook[1]

Received: 1 June 2020 / Accepted: 28 December 2020 / Published online: 3 February 2021

Keywords Uniaxial compressive strength · Brazilian tensile strength · P-wave and S-wave velocities · Elastic properties · Argillites

List of Symbols

L	Sample length
t	Travel time
V_p	P-wave velocity
V_s	S-wave velocity
E_s	Static Young's modulus
E_d	Dynamic Young's modulus
v_s	Static Poisson's ratio
v_d	Static Poisson's ratio
Φ	Porosity
ρ_B	Bulk density
UCS	Uniaxial compressive strength
TS	Tensile strength
Si	Silica
Cal	Carbonate
Clay	Clay

1 Introduction

Argillites are indurated mudstones and have relatively high strength and low permeability. These rocks are: often used for aggregates in the construction industry, used as armour rock for sea walls, good sites for the waste repository (e.g. Cuisinier et al. 2009; Jia et al. 2009; Zhang et al. 2014), and unconventional petroleum reservoirs provided that the organic content is high (e.g. Rodnikova et al. 1968). In the mining of most rocks including argillites, several engineering issues are encountered, such as rock fracturing around mining pits and the support and control of the fractured rock masses, during drilling, blasting, and tunnelling (e.g. Aladejare 2020). The Uniaxial compressive strength (UCS) and tensile strength are important prerequisite parameters in the engineering design to minimize these issues (e.g. Ng et al. 2015). The lack of these data will result in poor engineering design that can lead to the collapse of the mining and tunnelling sites. Therefore them is imperative to quantify the UCS and tensile strength by direct measurement or estimating it from other available data such as velocity, and elastic properties.

The UCS measurement can be time-consuming, expensive and impossible, especially for rocks that has well developed foliation and those that are highly fractured. The challenging aspect of determining the UCS is in the sample preparation, as the measurement requires sample with a length-to-diameter ratio (L/D) of 2.5–3 and their ends has to be parallel within ± 0.02 mm in accordance to ISRM (1983) standards. The Brazilian test, which is the most common indirect method used to measure the tensile strength, requires a circular disk with a thickness-to-diameter ratio (t/D) between 0.2 and 0.75 (ASTM D3967 2008). The preparation of circular disks is much easier to achieve compared to the sample dimensions required for UCS. In view of the fact that highly fractured rocks are unsuitable and high-quality rock core sample required for the UCS test are unavailable (Karaman et al. 2015; Ribeiro et al. 2016), empirical equations with a strong correlation will be more practical and efficient to estimate the UCS (Nazir et al. 2013).

There are various studies in the literature proposing relationships between UCS and tensile strength, UCS and velocities, and UCS and elastic properties on different rock types but no such relationships exist for argillites to the authors' knowledge (e.g. Arslan et al. 2008; Çobanoğlu and Çelik

✉ O. O. Blake
oshaine.blake@sta.uwi.edu

[1] Petroleum Geoscience, Department of Chemical Engineering, University of the West Indies, St. Augustine, Trinidad and Tobago

2008; Azimian et al. 2014; Najibi et al. 2015). The aim is to measure the UCS and indirect tensile (Brazilian) strength of argillites from the Naparima Hill Formation and correlate these results with P- and S-wave velocities, and static and dynamic elastic properties results of the same sample locations that were reported by Blake et al. (2020). These argillites have varying mineralogical composition and a wide range of porosity (Iyare et al. 2020). This study will also investigate how porosity, density, and mineral composition influence the UCS and tensile strength of the Naparima Hill Formation argillites.

2 Laboratory Measurements

2.1 Sample Preparation

In-situ block samples were extracted from the Naparima Hill Formation outcrop, Trinidad, at seven different locations (Fig. 1). These locations are representatives of four different lithofacies that were identified by Iyare et al. (2020): (a) Siliceous calcareous mudstones (location NHS7); (b) Calcareous mudstones interbedded with black chert (locations NHS1, NHS3, NHS4 and NHS14); (c) Carbonate rich mudstones with nodular chert (location NHS13); and (d) Siliceous mudstones (location NHS10). Iyare et al. (2020) revealed that these rocks have been subjected to diagenetic alteration such as pressure solution, mechanical compaction, cementation, and replacement of framework grains (Fig. 2). The late phase of uplift of the Formation, causes an uplift-induced residual strain to be released. Consequently, late-stage open microfractures were introduced in the Formation. Evidence of these microfractures are seen in thin section analysis of locations NHS13 (lithofacies c) and NHS14 (lithofacies b) (see Fig. 2f and g).

Cylindrical and circular disk samples of 20 mm diameter were plugged from the block samples. The mudstones are highly indurated with poor fissility and as such, are referred to as argillite. These argillites have similar lithofacies and porosities as siliceous argillites within locations including Monterey Formation, California, USA; Pillow Basalt Ridge facies, British Columbia, Canada; Viqueque Formation, Timor Leste; Freshwater Point Formation, Newfoundland, Canada; Red Rocks, Wellington, New Zealand; Bentong-Raub suture zone, Malaysia; and south Sakhalin-Hokkaido geosyncline, Hokkaido Island, Japan (Rodnikova et al. 1968; Misra 1971; Yurochko 1982; Snyder et al. 1983; Roser and Grapes 1990; Spiller 1996; Barresi et al. 2004; Haig and Bandini 2013).

All block samples were plugged such that their axis were perpendicular to the bedding of the outcrop. Cylindrical samples with L/D ratio of 2.5–3.0 were prepared according to ISRM (1983) standards for the UCS test. The circular disk samples were prepared with a t/D ratio of 0.2–0.75, according to ASTM D3967 (2008) standard, for the Brazilian tensile strength test. The ends of all the samples were trimmed and further flattened to strict tolerances (±0.02 mm) so that both ends were parallel to each other. The samples were dried at 50 °C in an oven for at least 48–72 h and cooled to room temperature before testing. For each location, four samples were prepared for the UCS test and ten samples were used to carry out the Brazilian test to obtain a meaningful average.

2.2 UCS test and Brazilian test

The UCS and Brazilian tests were carried out at the Geomechanics Laboratory, the University of West Indies using a servo-controlled triaxial apparatus (Fig. 3). The confining fluid was removed from the vessel and the confining pressure pipes were vented to atmospheric pressure. Hence, no confining pressure was applied and therefore intermediate principal stress (σ_2) and minimum principal stress (σ_3) are equal to zero. The samples were loaded at a constant stress rate of 0. 5 MPa/s in accordance with *ASTM D7012–14* (2014) until failure occurred. The maximum force load (F) sustained by the sample was recorded and used in conjunction with its cross-sectional area (A) to calculate the UCS.

$$UCS = \frac{F}{A} \tag{1}$$

where the force (F) is in N and the cross-sectional area (A) in m^2.

The apparatus was modified to conduct Brazilian testing. A steel cradle housing was fixed to the top thread of the pressure vessel (see Fig. 3e). The disk samples were placed between curved loading platens (see Fig. 3f). The radius of the curved platens is 1.5 times the sample radius, which adhered to the ISRM (1978) standards. A continuously increasing compressive load was applied at a rate of approximately 156 N/s, which made the weakest samples failed between 15 and 30 s (ISRM 1978). The tensile strength, TS in MPa, was calculated from the maximum recorded applied load (F) at failure, and the diameter (D) and thickness (t) of the sample according to:

$$TS = \frac{2F}{\pi Dt} \tag{2}$$

where the force (F) is in N, the diameter (D) in mm, and the thickness (t) in mm.

2.3 P- and S-wave Velocities, and Static and Dynamic Elastic Properties

The data sets used in this study are those reported in Blake et al. (2020). We briefly describe the methodology here for the context of this contribution. Sample plugs were taken

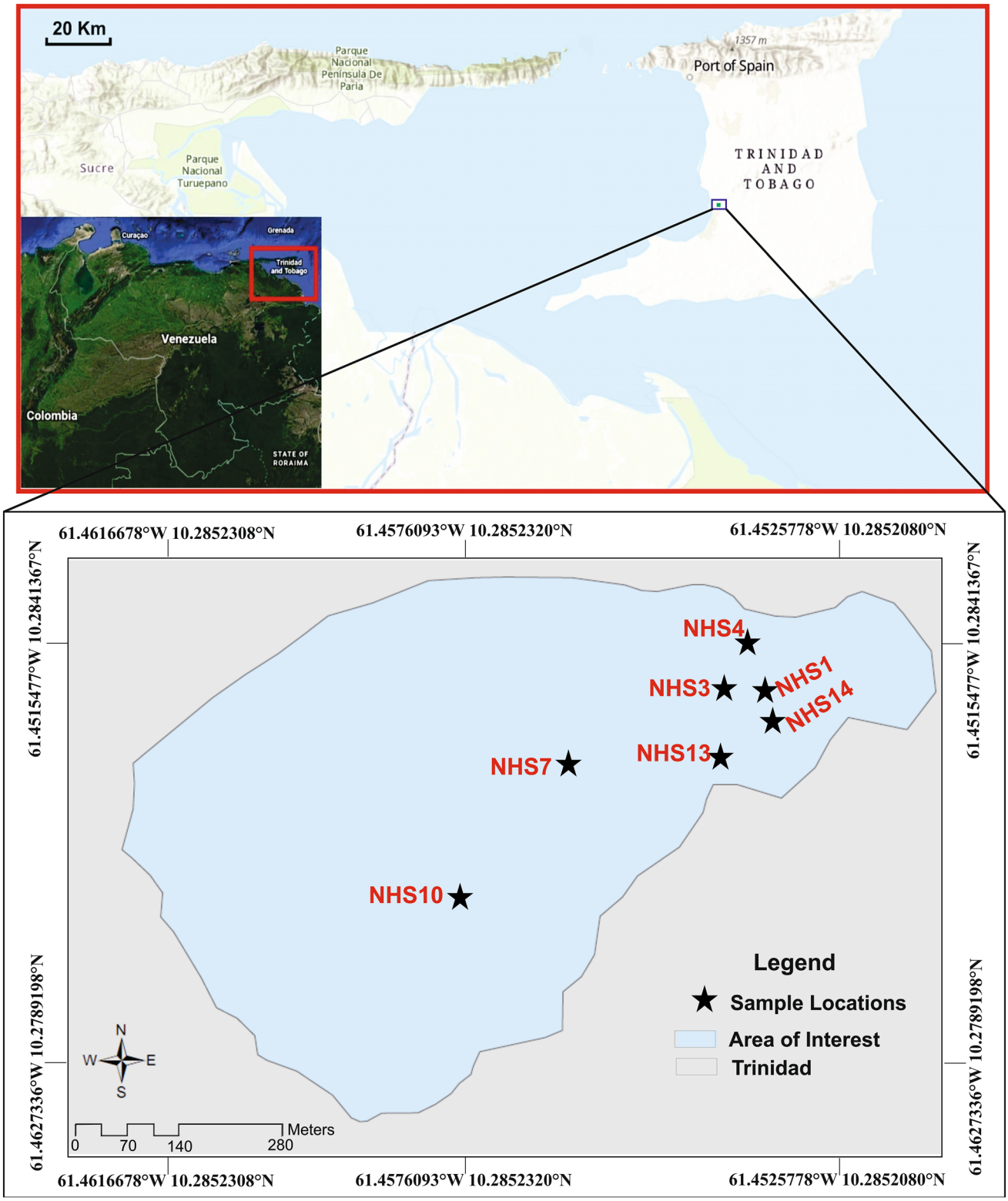

Fig. 1 Study area showing the location of the Naparima Hill Formation outcrop in Trinidad and the sample locations (NHS1, NHS3, NSH4, NSH7, NSH10, NSH13 and NHS14)

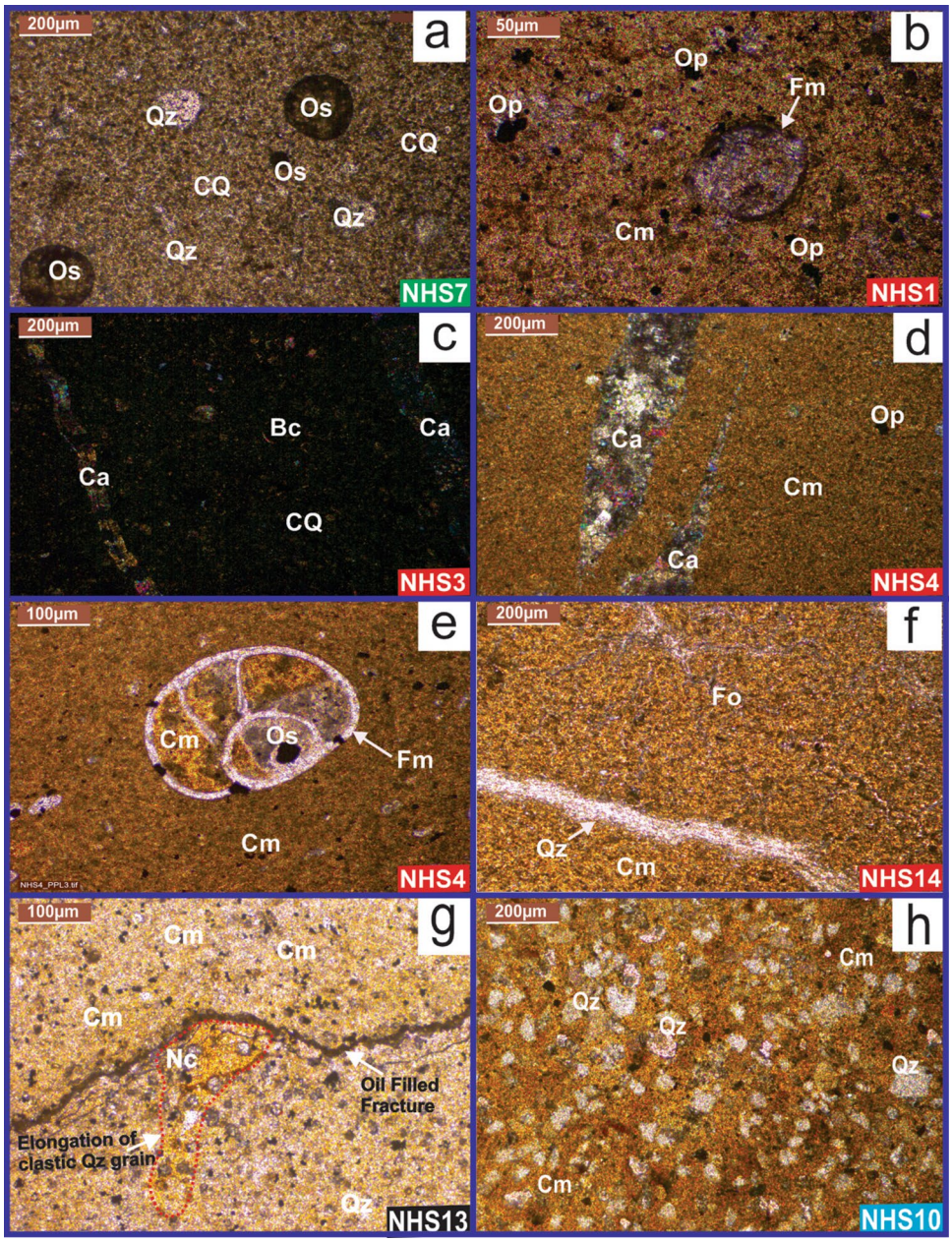

Fig. 2 Thin section images of the sampled outcrop locations (modified from Iyare et al. 2020). **a** NHS7; **b–f** NHS1, NHS3, NHS4, and NHS14; **g** NHS13 and **h** NHS10. The lithofacies are color coded: Lithofacies *a* = green; Lithofacies *b* = red; Lithofacies *c* = black; and Lithofacies *d* = blue. *Qz* Quartz, *Cm* Chert matrix, *Nc* Nodular Chert, *Op* Oil particle, *Ca* Calcite filled fracture, *CQ* Calcite-Quartz matrix, *Fo* Oil-filled fracture, *Os* Oil stain, *Fm* Foraminifera, *Bc* Bioclasts (color figure online)

from the same sample blocks that were used to determine the UCS and tensile strength. The plugs were also taken perpendicular to the outcrop bedding. All tests were conducted under the same dried conditions. The length to diameter ratio is approximately 2.5 with a diameter of 20 mm. Axial and radial strain gauges glued in the central region of the samples were used to monitor the axial and radial deformation. P- and S-wave piezoelectric ceramics, with the frequency of 1.5 MHz, at the top and bottom of the sample are used to generate and record the P- and S-waves travelling along the axis of the sample. An axial stress of less than 10 MPa was applied to couple the sample and loading platens to obtain measurable P- and S-waveforms. P- and S- wave velocities are determined as the length of the sample (L) divided by the travel time of the waves (t), corrected for the change in length due to the applied stress:

$$V_p or V_s = L/t \tag{3}$$

where V_p is the P-wave velocity and V_s is the S-wave velocity.

For elastic properties measurements, the samples were loaded up to 25% of their failure strength. The axial and radial stress-strain curves were differentiated at 20% of the failure strength to give the static tangent Young's modulus (E_s) and Poisson's ratio (v_s). P- and S-wave velocities measurements

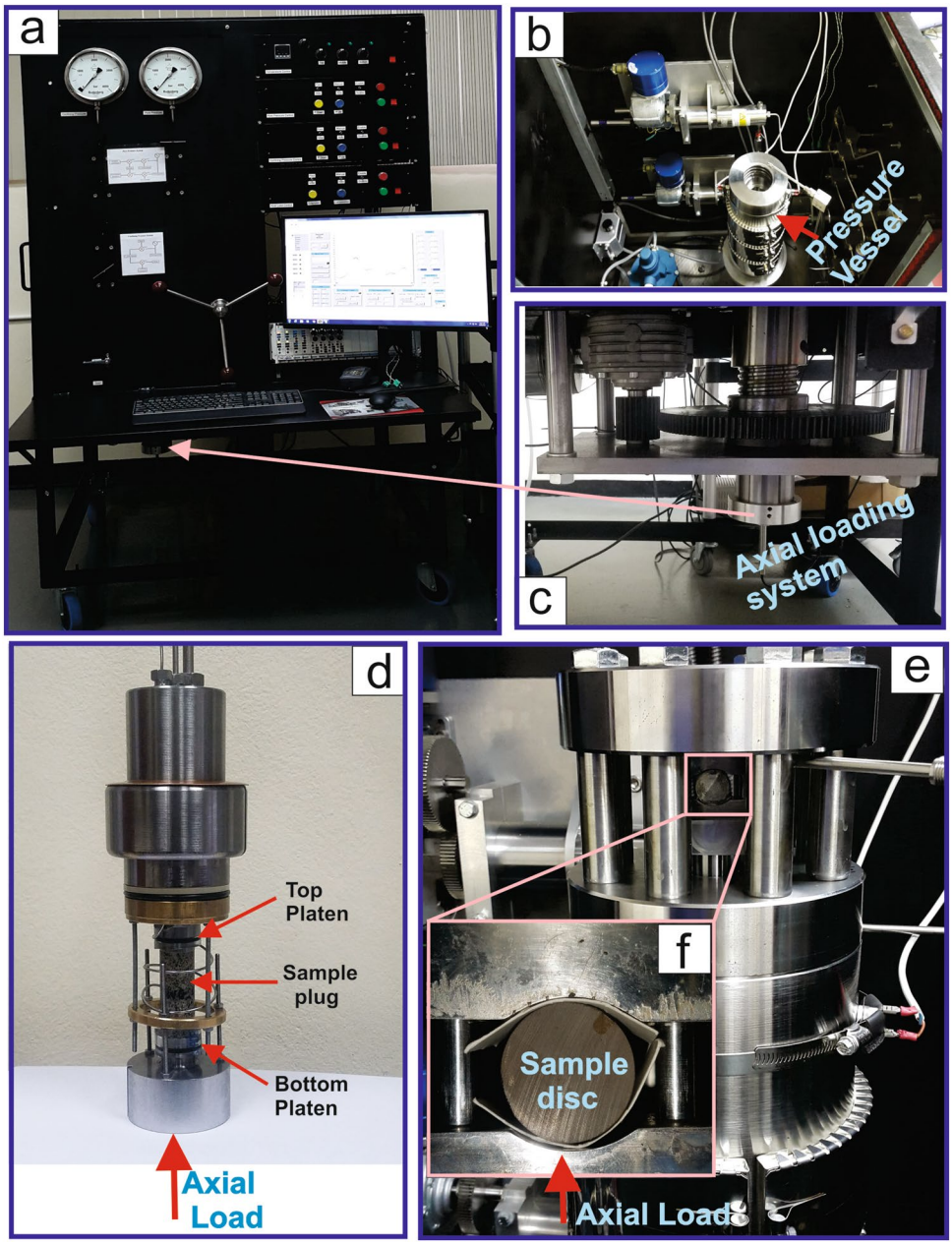

Fig. 3 Testing apparatus. **a** Front view of the triaxial apparatus. **b** Inside view of the triaxial apparatus. **c** Axial loading system. **d** Uniaxial compression test set up in the sample assembly. The top platen of the sample assembly is fixed when the assembly is placed inside the pressure vessel. **e** Indirect (Brazilian) tensile test set up showing the steel cradle housing. **f** Curve loading platens. Note: No confining fluid was applied to confine the sample. Therefore, all test were unconfined

were also taken at 20% of the failure strength from which the dynamic Young's modulus (E_d) and Poisson's ratio (ν_d) were calculated using the equations:

$$E_d = \frac{\rho V_s^2\left(3V_p^2 - 4V_s^2\right)}{V_p^2 - V_s^2} \tag{4}$$

$$\nu_d = \frac{V_p^2 - 2V_s^2}{2(V_p^2 - V_s^2)} \tag{5}$$

The change in the density, using the volumetric strain (two multiplied by the radial strain, plus the axial strain), were also taken into consideration in the calculation of the dynamic elastic properties.

3 Results

The mechanical and acoustic properties of the argillites are presented in Table 1. Lithofacies *a* has the lowest UCS and tensile strength of 44 MPa and 10 MPa, respectively. Lithofacies *b* which was sampled from four locations (NHS1, NHS3, NHS4, and NHS14) has UCS ranging from 126 to 210 MPa

and tensile strength of 20–28 MPa. Lithofacies *c* has the highest tensile strength of 36 MPa. The ratio of UCS to tensile strength shows no clear trend with lithofacies and ranges from 4.4 to 8. Figure 4 shows that locations NHS3, NHS4, NHS13 and NHS14 have a large standard deviation for the UCS. Large standard deviation in the tensile strength is observed for locations NHS4, NHS13 and NHS14. Lithofacies *a* has the lowest velocities (P- wave velocity of 2551 m/s, S-wave velocity of 1801 m/s). The highest velocities are from lithofacies *c* (P-wave velocity of 4689, S-wave velocity of 2852). The dynamic Young's modulus are greater than the static Young's modulus. The static and dynamic Poisson's ratios are approximately equal. Lithofacies *a* has the lowest Young's modulus and Poisson's ratio ($E_s = 6.29$ GPa and $E_d = 12.7$ GPa, $\nu_s = 0.11$ and $\nu_d = 0.02$) and lithofacies *c* has the highest Young's modulus and Poisson's ratio ($E_s = 36.95$ GPa and $E_d = 47.57$ GPa, $\nu_s = 0.20$ and $\nu_d = 0.21$).

Figure 5 shows the correlations between the UCS and the tensile strength of the seven different locations. There is a strong power-law correlation between the UCS and tensile strength with a high coefficient of determination (R^2) of 0.87. The equation of the line is:

$$UCS = 5.31TS^{1.06} \tag{6}$$

where the units of UCS and TS are in MPa. The correlations between UCS and velocities, and UCS and elastic properties of the seven different locations are shown in Fig. 6. There exist strong linear corrections with R^2 greater than 0.85. The equations and R^2 of the lines are:

$$UCS = 0.076V_p - 158.85,\ R^2 = 0.94 \tag{7}$$

$$UCS = 0.157V_s - 249.83,\ R^2 = 0.92 \tag{8}$$

$$UCS = 4.70E_d - 14.814,\ R^2 = 0.90 \tag{9}$$

$$UCS = 783.31\nu_d - 16.64,\ R^2 = 0.89 \tag{10}$$

$$UCS = 4.96E_s + 27.52,\ R^2 = 0.85 \tag{11}$$

$$UCS = 1354.60\nu_s - 97.45,\ R^2 = 0.97 \tag{12}$$

where the units of UCS is in MPa, V_p and V_s are in m/s, E_d and E_s are in GPa, and ν_s *and* ν_d are unit less. There also exist strong linear correlations with R^2 greater than 0.74 when the tensile strength (TS) is correlated with velocities and elastic properties (see Fig. 7). The equations and R^2 of the lines are:

$$TS = 0.012V_p - 23.23,\ R^2 = 0.86 \tag{13}$$

$$TS = 0.024V_s - 36.67,\ R^2 = 0.83 \tag{14}$$

$$TS = 0.75E_d - 2.55,\ R^2 = 0.90 \tag{15}$$

$$TS = 115.28\nu_d + 3.75,\ R^2 = 0.76 \tag{16}$$

$$TS = 0.795E_s - 4.02,\ R^2 = 0.86 \tag{17}$$

$$TS = 187.66\nu_s - 11.05,\ R^2 = 0.74 \tag{18}$$

where the units of TS is in MPa, V_p and V_s are in m/s, E_d and E_s are in GPa, and ν_s *and* ν_d are unit less.

Table 1 Uniaxial compressive strength, tensile strength, elastic properties, and P- and S-wave velocities of the argillites

Lithofacies	Outcrop locations	Uniaxial compressive strength (MPa)	Tensile strength (MPa)	P-wave velocity (m/s)	S-wave velocity (m/s)	Static Young's modulus (GPa)	Static Poisson's ratio	Dynamic Young's modulus (GPa)	Dynamic Poisson's ratio
Lithofacies *a*	NHS7	44 ± 1.7	10 ± 1.7	2550.55	1800.72	6.29	0.11	12.70	0.02
Lithofacies *b*	NHS1	126 ± 16.1	20 ± 4.3	3683.41	2351.46	16.03	0.18	27.43	0.16
	NHS3	135 ± 41.8	21 ± 4.4	3948.30	2422.69	16.51	0.16	30.10	0.18
	NHS4	210 ± 60.4	28 ± 7.9	4533.70	2797.33	31.98	0.22	43.63	0.20
	NHS14	160 ± 31.8	20 ± 6.2	4171.65	2585.89	26.20	0.19	34.35	0.18
Lithofacies *c*	NHS13	180 ± 47.2	36 ± 11.3	3114.95	2162.27	11.93	0.12	21.46	0.07
Lithofacies *d*	NHS10	63 ± 6.2	9 ± 0.8	4688.69	2851.60	36.95	0.20	47.57	0.21

The P- and S-wave velocities, static and dynamic Young's moduli and Poisson's ratio were obtained from Blake et al. (2020). We included the following sentences in Table 1 legend: Four plug samples per location were used to determine an average of the uniaxial compressive strength. Ten circular disk samples per location were used to determine an average of the Tensile strength. One plug per location was used to simultaneously measure P- and S-wave velocities (from which dynamic elastic properties were derived) and static elastic properties

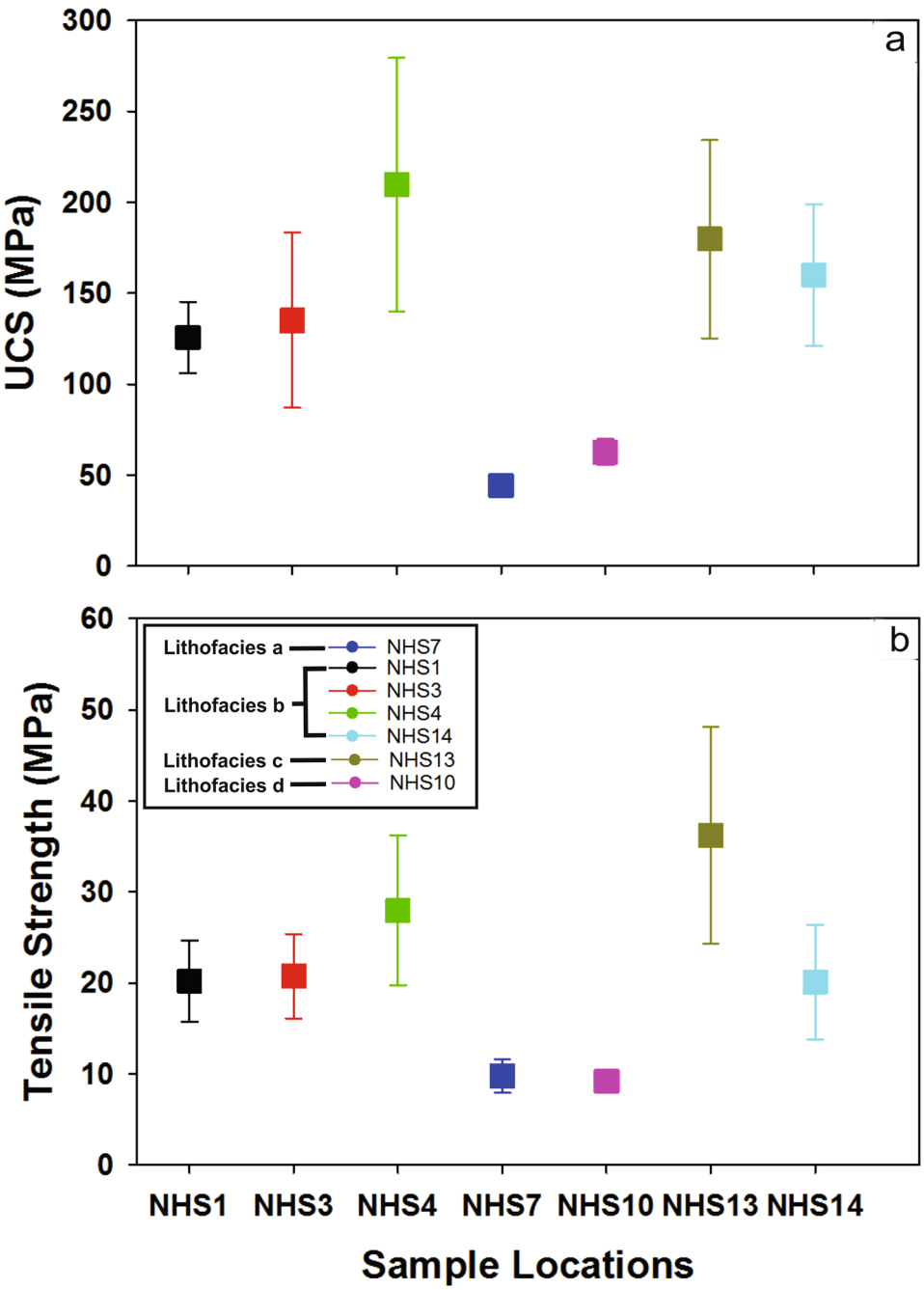

Fig. 4 UCS **a** and tensile strength **b** for all locations. Four UCS tests and ten tensile strength tests were carried out at each location. Error bar shows standard deviation

4 Discussion

Rock properties such as porosity, density and mineral composition can influence the strength of the rock (e.g. Kahraman et al. 2005). The mineral composition of the lithofacies is presented in Table 2. The grain size of lithofacies *a* to lithofacies *d* ranged from fine-grained to very fine-grained, and the mineral composition varies with respect to silica, carbonate and clay content (Iyare et al. 2020). Table 2 shows that carbonate content are only present in lithofacies *b* and lithofacies *c*. The carbonate in these lithofacies, have been reported as calcite cementation, which is a diagenetic event altering the fabric of the rocks in Naparima Hill Formation (Iyare et al. 2020). Carbonate cementation has been reported to decrease porosity and increase cohesion in sediment which then increases rock strength substantially (e.g. Sample 1990).

The correlations between the strength parameters and porosity, density and mineral compositions are presented to understand how these variables influence the strength parameters. Iyare et al. (2020) reported dry bulk density (ρ_B) and porosity (Φ) of the Naparima Hill Formation

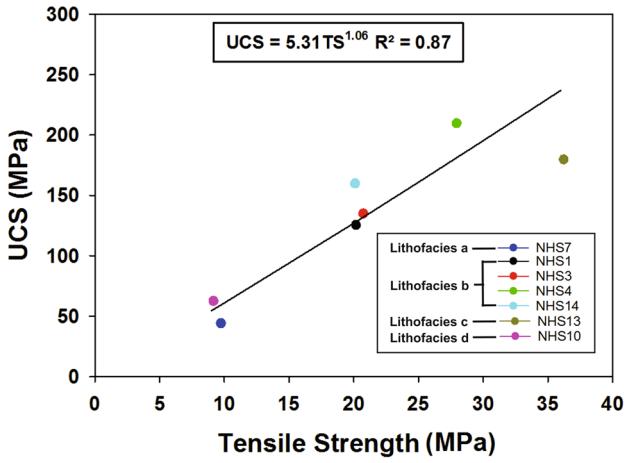

Fig. 5 Correlation between UCS and tensile strength

outcrop lithofacies to vary from 1841 to 2347 kg/m^3 and 5.9 to 30.8%, respectively (see Table 2). The UCS and tensile strength are seen to generally decrease with an increase in Φ and increase with an increase in ρ_B (Fig. 8). This is consistent with several published reports (Palchik and Hatzor 2004; Baud et al. 2014; Jamshidi et al. 2018). The correlation between Φ and UCS appears to be moderate with an R^2 of 0.70, while the correlation between ρ_B and UCS is weak with an R^2 of 0.49. The correlations obtained between Φ and tensile strength, and ρ_B and tensile strength are also very weak with R^2 of 0.47 and R^2 of 0.24, respectively. The poor correlations corroborate with findings from Inoue and Ohomi (1981), Lashkaripour and Passaris (1995), Inoue and Ohomi (1981) and Karaman et al. (2015).

A closer look at the data in Fig. 8c and d, shows lithofacies c having the highest tensile strength despite not having the lowest porosity and highest density (see Table 2). The results in Table 1 suggest that lithofacies *c* has the highest standard deviation of the tensile strength. This is because lithofacies *c* is highly heterogeneous. Sampling of rocks in lithofacies *c* may encounter some rocks that are predominantly silica or cemented with calcite, which will give low or high tensile strength values. The heterogeneity will be more noticeable in the tensile strength than in the UCS because the length of sample (circular disk) for tensile strength test is very short compared to the length of samples required for UCS test. It is highly probable that the circular disks sampled either silica or carbonate-rich zones, whereas the UCS plugs will sample both zones.

Figure 9 shows the variation of the UCS and tensile strength with mineral content. It is observed that UCS and tensile strength show a negative linear correlation with the percentage composition of silica (Fig. 9a and d), and a positive linear correlation with the percentage composition of carbonate (Fig. 9b and e). The variation of percentage composition of clay with UCS and tensile strength is shown in Fig. 9c and f. The data is scattered and fitting a linear function to it, show poor R^2 of 0.43 and

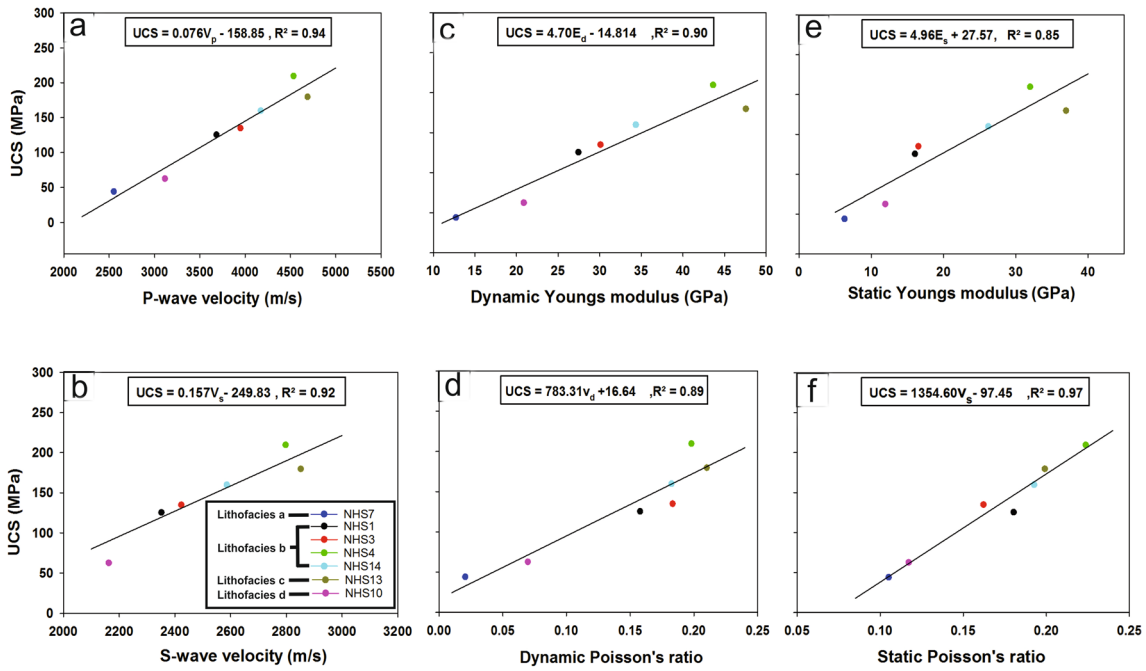

Fig. 6 Correlation between: UCS and P-wave velocity (**a**); UCS and S-wave velocity (**b**); UCS and dynamic Young's modulus (**c**); UCS and dynamic Poisson's ratio (**d**); UCS and static Young's modulus (**e**); and UCS and static Poisson's ratio (**f**)

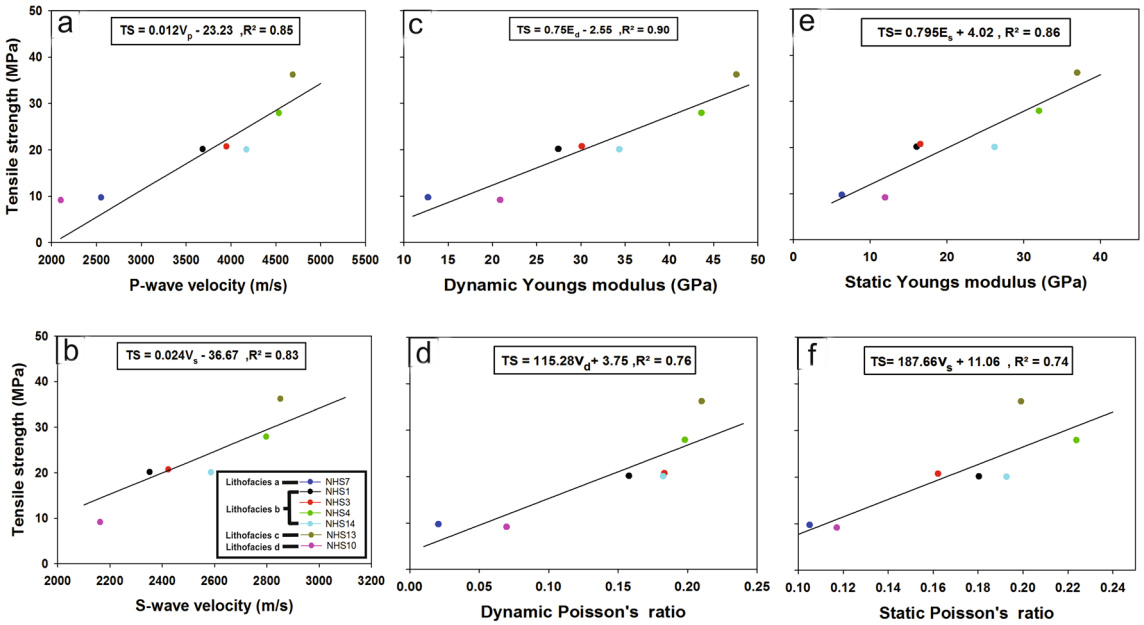

Fig. 7 Correlation between: tensile strength against P-wave velocity (**a**); tensile strength and S-wave velocity (**b**); tensile strength and dynamic Young's modulus (**c**); tensile strength and dynamic Poisson's ratio (**d**); tensile strength and static Young's modulus (**e**); and tensile strength and static Poisson's ratio (**f**)

Table 2 Summary of the dry bulk density, porosity and mineral compositions of the argillites (Adapted from Iyare et al. 2020)

Lithofacies	Outcrop locations	Dry bulk density (ρ_B) (Kg/m^3)	Porosity (Φ) (%)	Silica content (Wt. %)	Carbonate content (Wt. %)	Clay content (Wt. %)
Lithofacies *a*	NHS7	1841 ± 7.8	30.8 ± 0.2	94	0	6
Lithofacies *b*	NHS1	2153 ± 15.4	14.0 ± 0.7	77	14	7
	NHS3	2105 ± 8.4	14.2 ± 0.2	77	12	8
	NHS4	2347 ± 97.9	5.9 ± 2.6	62	34	2
	NHS14	2113 ± 26.2	16.0 ± 0.2	75	18	6
Lithofacies *c*	NHS13	2028 ± 27.1	18.2 ± 1.2	49	39	2
Lithofacies *d*	NHS10	2101 ± 14.4	20.9 ± 0.6	93	0	7

0.55 with the UCS and tensile strength, respectively. Furthermore, the clay content is very low in these samples. The correlations in Fig. 9a and d suggest that decreasing the percentage composition of silica and increasing the percentage composition of carbonate increases the UCS and tensile strength. We observed that while the porosity decreases, the amount of carbonate minerals increases, which is likely to be filling the pore spaces and fractures. It is highly possible that the actual amount of silica within the samples remains fairly constant. Therefore, an increase in the carbonate will only reflect a reduction in the percentage composition of silica.

5 Conclusion

The uniaxial compressive strength and indirect tensile (Brazilian) strength of the argillites in the Naparima Hill Formation were studied using dry samples that were cored perpendicular to the outcrop bedding. The strength of these argillites are influenced by porosity and carbonate cementation. As the pore space of the rocks are filled with carbonate, the porosity decreases, the density increases, and thus the strength of the argillites increases.

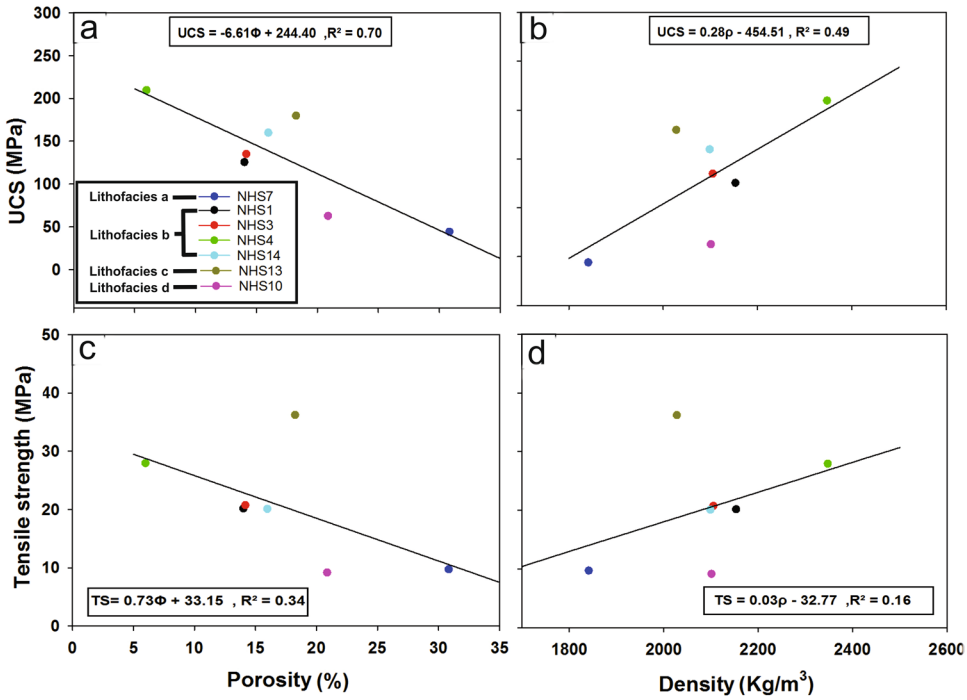

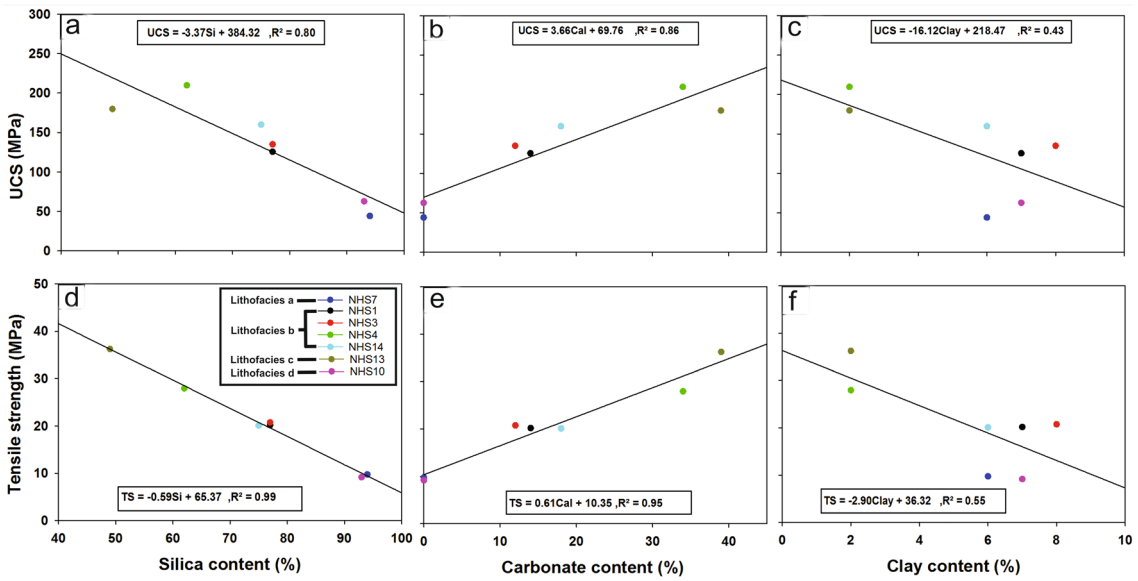

Fig. 8 Correlation between: **a** UCS and porosity (Φ), **b** UCS and density (ρ), **c** tensile strength and porosity (Φ), and **d** tensile strength and density (ρ)

Fig. 9 Influence of mineral composition on the UCS and tensile strength: **a** silica content on UCS; **b** carbonate content on UCS; **c** clay content on UCS; **d** silica content on tensile strength; **e** carbonate content on tensile strength and **f** clay content on tensile strength. *UCS* uniaxial compressive strength, *TS* tensile strength, *Si* silica content, *Cal* carbonate content, *Clay* clay content

Empirical relationships that relate mechanical and seismic transport properties to UCS are uncommon for argillites. We established a strong power-law relationship between the UCS and tensile strength, and strong linear relationships between the UCS and velocities (P- and S-wave), and UCS and elastic properties (static and dynamic Young's moduli and Poisson's ratio). These results suggest that the Brazilian tensile strength and P- and S-wave velocities, as a less expensive, quick, and practical methods, can be reliably used to determine the UCS.

Acknowledgements We would like to thank the Ministry of Energy and Energy Industries, Trinidad and Tobago, Engineering Institute, Faculty of Engineering, and Campus Research and Publication Fund

Committee, University of the West Indies, St. Augustine Campus, for funding this research.

Compliance with Ethical Standards

Conflict of interest The authors declare that they have no conflict of interest.

References

Aladejare AE (2020) Evaluation of empirical estimation of uniaxial compressive strength of rock using measurements from index and physical tests. J Rock Mech Geotech Eng 12(2):256–268. https://doi.org/10.1016/j.jrmge.2019.08.001

Arslan A, Koca Y, Aydogmus T, Klapperich H, Yılmaz H (2008) Correlation of unconfined compressive strength with young's modulus and poisson's ratio in gypsum from sivas (Turkey). Rock Mech Rock Eng 41:941–950. https://doi.org/10.1007/s00603-007-0145-8

ASTM D3967, S. (2008) Standard test method for splitting tensile strength of intact rock core specimens (ASTM D3967–08). Annual Book of ASTM Standards, American Society for Testing and Materials, West Conshohocken

ASTM D7012–14, S. (2014) Standard test methods for compressive strength and elastic moduli of intact rock core specimens under varying states of stress and temperatures. ASTM International, West Conshohocken

Azimian A, Ajalloeian R, Fatehi L (2014) An empirical correlation of uniaxial compressive strength with P-wave velocity and point load strength index on marly rocks using statistical method. Geotech Geol Eng 32(1):205–214

Barresi T, Nelson J, Alldrick D, Dostal J (2004) Pillow basalt ridge facies: detailed mapping of eskay creek-equivalent stratigraphy in northwestern british columbia. Geol Fieldwork 2004:2005

Baud P, Wong T-F, Zhu W (2014) Effects of porosity and crack density on the compressive strength of rocks. Int J Rock Mech Min Sci 67:202–211. https://doi.org/10.1016/j.ijrmms.2013.08.031

Blake OO, Ramsook R, Faulkner DR, Iyare UC (2020) The effect of effective pressure on the relationship between static and dynamic young's moduli and poisson's ratio of naparima hill formation mudstones. Rock Mech Rock Eng. https://doi.org/10.1007/s00603-020-02140-0

Çobanoğlu İ, Çelik SB (2008) Estimation of uniaxial compressive strength from point load strength, schmidt hardness and P-wave velocity. Bull Eng Geol Env 67(4):491–498

Cuisinier O, Deneele D, Masrouri F (2009) Shear strength behaviour of compacted clayey soils percolated with an alkaline solution. Eng Geol 108(3–4):177–188

Haig DW, Bandini AN (2013) Middle Jurassic Radiolaria from a siliceous argillite block in a structural melange zone near Viqueque, Timor Leste: Paleogeographic implications. J Asian Earth Sci 75:71–81. https://doi.org/10.1016/j.jseaes.2013.06.008

Inoue, M., and M. Ohomi (1981), Relation Between Uniaxial Compressive Strength And Elastic Wave Velocity of Soft Rock, in ISRM International Symposium, edited, p. 5, International Society for Rock Mechanics and Rock Engineering, Tokyo, Japan.

ISRM (1978) Suggested methods for the quantitative description of discontinuities in rock masses. ISRM Int J Rock Mech Min Sci Geomech Abstr 15(6):319–368

ISRM (1983) Suggested methods for determining the strength of rock materials in triaxial compression: revised version. Int J Rock Mech Min Sci Geomech Abstr 20(6):285–290. https://doi.org/10.1016/0148-9062(83)90598-3

Iyare UC, Ramsook R, Blake OO, Faulkner DR (2020) Petrographical and petrophysical characterization of the late cretaceous naparima hill formation, central range, trinidad, West Indies. Int J Coal Geol 230:103592. https://doi.org/10.1016/j.coal.2020.103592

Jamshidi A, Zamanian H, Zarei Sahamieh R (2018) The effect of density and porosity on the correlation between uniaxial compressive strength and P-wave velocity. Rock Mech Rock Eng 51(4):1279–1286. https://doi.org/10.1007/s00603-017-1379-8

Jia Y, Bian H, Duveau G, Su K, Shao J-F (2009) Numerical modelling of in situ behaviour of the callovo-oxfordian argillite subjected to the thermal loading. Eng Geol 109(3–4):262–272

Kahraman S, Gunaydin O, Fener M (2005) The effect of porosity on the relation between uniaxial compressive strength and point load index. Int J Rock Mech Min Sci 42:584–589. https://doi.org/10.1016/j.ijrmms.2005.02.004

Karaman K, Cihangir F, Ercikdi B, Kesimal A, Demirel S (2015) Utilization of the Brazilian test for estimating the uniaxial compressive strength and shear strength parameters. J S Afr Inst Min Metall 115:185–192. https://doi.org/10.17159/2411-9717/2015/v115n3a3

Lashkaripour, G. R., and E. K. S. Passaris (1995), Correlations Between Index Parameters And Mechanical Properties of Shales, in 8th ISRM Congress, edited, p. 5, International Society for Rock Mechanics and Rock Engineering, Tokyo, Japan

Misra S (1971) Stratigraphy and depositional history of late Precambrian coelenterate-bearing rocks, southeastern Newfoundland. Geol Soc Am Bull 82(4):979–988

Najibi AR, Ghafoori M, Lashkaripour GR, Asef MR (2015) Empirical relations between strength and static and dynamic elastic properties of Asmari and Sarvak limestones, two main oil reservoirs in Iran. J Petrol Sci Eng 126:78–82

Nazir R, Momeni E, Jahed Armaghani D, Mohd Amin M (2013) Correlation between unconfined compressive strength and indirect tensile strength of limestone rock samples. Electron J Geotech Eng 18:1737–1746

Ng I-T, Yuen K-V, Lau C-H (2015) Predictive model for uniaxial compressive strength for Grade III granitic rocks from Macao. Eng Geol 199:28–37. https://doi.org/10.1016/j.enggeo.2015.10.008

Palchik V, Hatzor YH (2004) The influence of porosity on tensile and compressive strength of porous chalks. Rock Mech Rock Eng 37:331–341. https://doi.org/10.1007/s00603-003-0020-1

Ribeiro PCPDS, MM Oliveira, P Nelson (2016) Correlation between Uniaxial Compressive Strength and Brazilian Tensile Strength Using Different Rock Types, in *ISRM VII Brazilian Symposium on Rock Mechanics - SBMR 2016*, edited, p. 8, International Society for Rock Mechanics and Rock Engineering, Belo Horizonte, Minas Gerais, Brazil

Rodnikova R, Sevost'yanov K, Taboyakov AY (1968) Structural-formation connection between southern Sakhalin Island and Hokkaido Island in relation to hydrocarbon potential. Int Geol Rev 10(7):749–760

Roser B, Grapes R (1990) Geochemistry of a metabasite—chert—coloured-argillite—turbidite association at Red Rocks, Wellington, New Zealand. NZ J Geol Geophys 33(2):181–191

Sample JC (1990) The effect of carbonate cementation of underthrust sediments on deformation styles during underplating. J Geophy Res Solid Earth 95(B6):9111–9121. https://doi.org/10.1029/JB095iB06p09111

Snyder WS, Brueckner HK, Schweickert RA (1983) Deformational styles in the Monterey Formation and other siliceous sedimentary rocks. In: Isaacs CM, Garrison RE (eds) Petroleum generation and occurrence in the Miocene Monterey Formation. Pacific Section, Society of Economic Paleontologists and Mineralogists, Los Angeles, California, pp 151–170

Spiller FC (1996) Late Paleozoic radiolarians from the Bentong-Raub suture zone Peninsular Malaysia. Island Arc 5(2):91–103
Yurochko A (1982) Composition and physical properties of siliceous and clay-siliceous reservoir rock in the Okruzhnoye oil field (Sakhalin Island). Int Geol Rev 24(11):1263–1268
Zhang F, Hu D, Xie S, Shao J-F (2014) Influences of temperature and water content on mechanical property of argillite. Eur J Environ Civil Eng 18(2):173–189